iScience

CellPress
OPEN ACCESS

Article

Biodegradable metal-organic framework MIL-88A for triboelectric nanogenerator

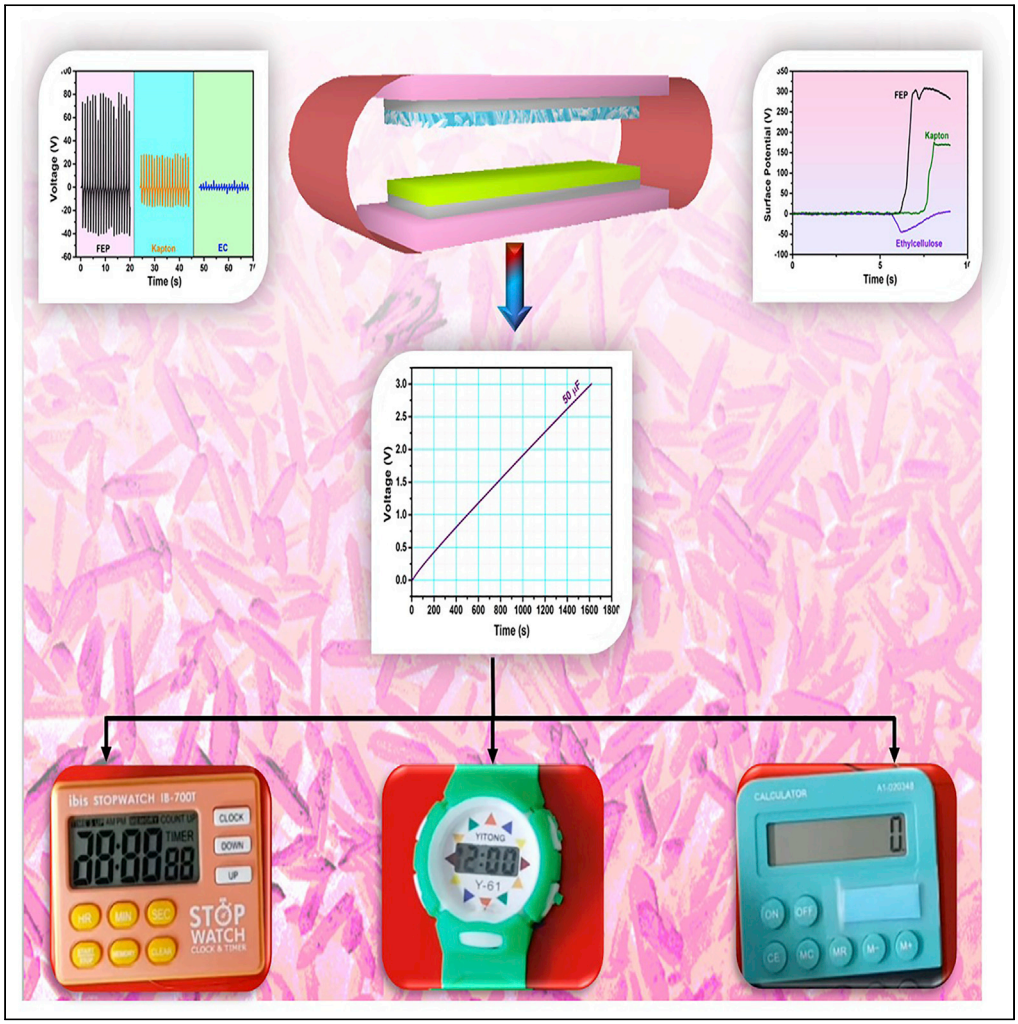

Gaurav Khandelwal, Nirmal Prashanth Maria Joseph Raj, Venkateswaran Vivekananthan, Sang-Jae Kim

kimsangj@jejunu.ac.kr

HIGHLIGHTS

Biodegradable MIL-88A behave as positive material concerning FEP and Kapton

MIL-TENG produces an output of 80 V and 2.2 μA

MIL-TENG demonstrated for biomechanical energy harvesting

Numerous low-power electronics are powered using MIL-TENG via a capacitor

Khandelwal et al., iScience 24, 102064
February 19, 2021
https://doi.org/10.1016/j.isci.2021.102064

iScience

CellPress
OPEN ACCESS

Article

Biodegradable metal-organic framework MIL-88A for triboelectric nanogenerator

Gaurav Khandelwal,[1] Nirmal Prashanth Maria Joseph Raj,[1] Venkateswaran Vivekananthan,[1] and Sang-Jae Kim[1,2,*]

SUMMARY

Metal-organic frameworks (MOFs) are multifunctional materials with a unique advantage of high porosity and surface area and size tunability and can be modified without altering the topology. The interesting and desirable properties of MOFs led to their exploration for the triboelectric nanogenerator. Herein, a biodegradable MOF MIL-88A for TENG (MIL-TENG) is reported. MIL-88A can be easily synthesized by coordinating iron chloride and fumaric acid in water, thus offering eco-friendly synthesis. Various materials are selected as opposite layers to MIL-88A to analyze triboelectric behavior and performance. The MIL-TENG exhibits an output trend of $TENG_{EC}$ < $TENG_{Kapton}$ < $TENG_{FEP}$. The MIL-88A and FEP generated an output voltage of 80 V and an output current of 2.2 μA. The surface potential measurement and electrical output trend suggest the positive triboelectric behavior of MIL-88A concerning FEP and Kapton. The utilization of biomechanical motions and numerous low-rating electronics powered via a capacitor are demonstrated.

INTRODUCTION

The discovery of metal-organic frameworks (MOFs) goes back to a few decades. Since their discovery, many works were carried out related to the applications, synthesis, and properties of the MOFs. The MOFs are crystalline materials, with metal ion associated with the linker (imidazolates, carboxylates, phosphonates, etc.) (Liu et al., 2018; Furukawa et al., 2013). The MOFs are excellent candidates for many applications like catalysis, energy storage, gas separation, imaging, gas storage, drug delivery, etc. (Liu et al., 2018; Wang et al., 2016a, 2018; Furukawa et al., 2013; Baumann et al., 2019; Li et al., 2018). The wide range of MOF applications is due to their appealing properties like high surface area, uniform and flexible porosity, variety of topology, and so on (Furukawa et al., 2013). Nevertheless, the increased use of MOFs or nanoparticles is associated with environmental and health issues regarding the safety and their effect on the living systems.

Recently, MOFs are utilized for energy harvesting via triboelectric nanogenerator (TENG), combining the triboelectric effect and electrostatic induction (Khandelwal et al., 2019). The MOFs that have been utilized for TENG are zeolitic imidazole framework members, bromine-functionalized covalent organic framework, HKUST-1, etc. (Khandelwal et al., 2019, 2020a, 2020b; Wen et al., 2019; Zhai et al., 2020). The MOFs are added as a multifunctional material in triboelectric series and deliver good performance in various applications. The MOFs can behave as positive or negative triboelectric material depending on the functional group. The bromine-functionalized MOF produces high output with PVDF as the opposite layer compared with its non-bromine-containing counterparts due to enhanced charge transport capability (Zhai et al., 2020). Similarly, fluorinated MOF can behave as high tribonegative materials (Guo et al., 2020). The non-toxic MOFs with no harmful effects on the environment and biological systems are critical for sustainable development. The non-toxic MOFs can be used to extend MOF application for future TENG-based implantable devices and biodegradable sensors.

MIL-88A, composed of iron metal ion and fumaric acid as a ligand, is a non-toxic MOF (Wang et al., 2016a; Liu et al., 2018; Liao et al., 2019). The MIL-88A can be rapidly isolated by the liver and spleen (Baati et al., 2013). The MIL-88A sequestration does not induce any persistent toxicity, and organs remain functionally intact. Moreover, MIL-88A can be degraded into individual components, i.e., iron and fumaric acid. The fumaric acid was suggested to be utilized in the Krebs cycle rather than excreting out of the body

[1]Nanomaterials and System Lab, Faculty of Applied Energy Systems, Major of Mechatronics Engineering, Jeju National University, Jeju 690-756, South Korea

[2]Lead contact

*Correspondence: kimsangj@jejunu.ac.kr

https://doi.org/10.1016/j.isci.2021.102064

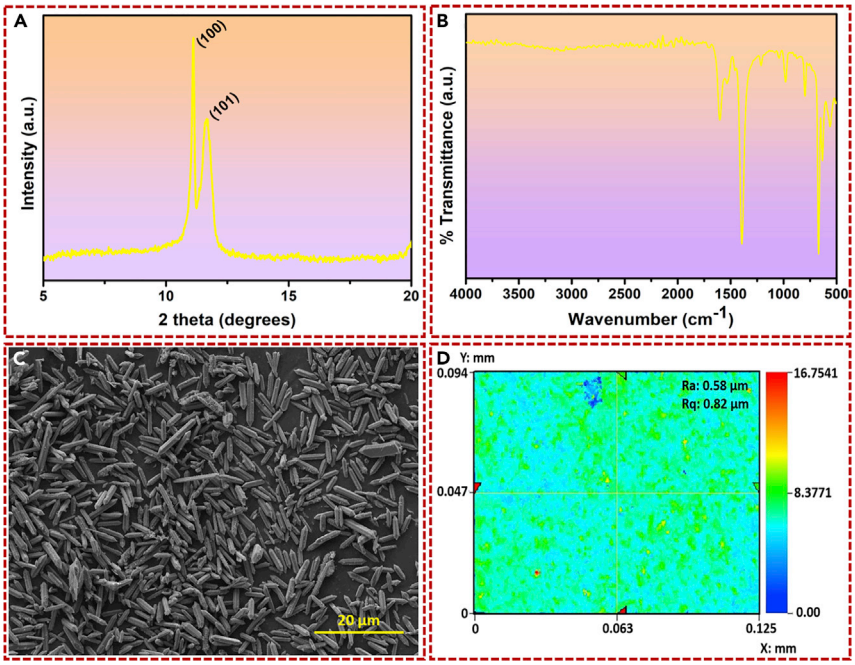

Figure 1. Structural and morphological characterization of MIL-88A

(A) XRD spectra of MIL-88A.

(B) FT-IR spectra of MIL-88A.

(C and D) (C) FE-SEM image revealing the rod-shape morphology of the synthesized MIL-88A and (D) 2D surface roughness profile image of MIL-88A.

(Baati et al., 2013). In this work, non-toxic MIL-88A microrods are reported for energy harvesting via coupling of contact electrification and electrostatic induction. The electrostatic surface potential measurement suggests the relative positive behavior of the MIL-88A. The MIL-TENG with FEP as opposite layer generated a maximum output voltage and current of 80 V and 2.2 μA, respectively. The electrical measurements reveal the detailed characteristics of MIL-TENG, suggesting that MIL-88A as a suitable non-toxic multifunctional material. Finally, the practical implementation of MIL-TENG is demonstrated by biomechanical energy harvesting and powering numerous electronics.

RESULTS AND DISCUSSION

Figure 1A confirms the crystalline structure of MIL-88A as revealed by X-ray diffraction (XRD). The 10.2° and 11.8° peaks corresponding to the presence of (100) and (101) phase suggest the formation of rod-like structures (Liao et al., 2019). Figure 1B depicts the Fourier transform infrared (FT-IR) spectrum of MIL-88A. The peaks at 1,396 and 1,603 cm^{-1} correspond to the symmetric and asymmetric vibration of the carboxyl group, respectively. The peak at 658 cm^{-1} is ascribed to the carbonyl group. The absence of significant broadband in the region 3,200–3,400 cm^{-1} suggests the absence of water (Durymanov et al., 2019). Figure 1C shows the field emission scanning electron microscope (FE-SEM) image of the MIL-88A, confirming the rod-like structures; in the diameter range of 0.7–1 μm and length in the range of 4–6 μm. The energy-dispersive spectroscopy (EDS) mapping confirms the presence of iron, carbon, and oxygen as expected for MIL-88A (Figure S1). The performance of TENG alters with the surface roughness (Lee et al., 2013; Jeong et al., 2014; Tang et al., 2014). Figure 1D illustrates the 2D surface profile of MIL-88A. The MIL-88A exhibits an average surface roughness (Ra) of 0.58 μm and root-mean-square roughness (Rq) of 0.82 μm. The optical profile of the coated layer does not match with the FE-SEM image. The 2D optical profile image was captured for the compactly pressed powder layer on the Al electrode. This leads to the compact arrangement of the nanorods, making it difficult to identify the boundaries precisely. The optical profilers are used to measure the surface roughness. The optical profiler lateral resolution is very poor, but they have an excellent vertical resolution, which is critical for the surface roughness measurement. The optical and 2D profile images to confirm the morphology were taken by drop-casting the dispersed sample on the Al foil. The optical and 2D profile images of dispersed samples are shown in Figure S2.

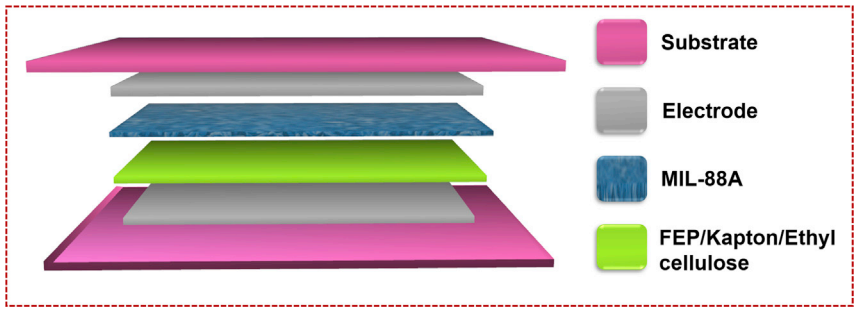

Figure 2. The 3D exploded view of MIL-TENG

Figure 2 shows the exploded 3D view of the MIL-TENG. The vertical contact-separation mode MIL-TENG is composed of MIL-88A and FEP (fluorinated ethylene propylene)/Kapton/EC (ethylcellulose) as an opposite layer. The aluminum (Al) tape with conducting adhesive was used as the electrode, and polyethylene terephthalate serves the substrate purpose.

Figure 3 shows the detailed electrical characteristics of the MIL-TENG. Figures 3A–3C depicts the voltage, current, and charge generated by MIL-TENG with FEP/Kapton/EC as the opposite layers. The FEP MIL-TENG generated the highest output voltage, current, and charge of 80 V, 2.2 μA, and 25 nC. The effect of the device size on the output of MIL-TENG is shown in Figure S3. The MIL-TENG follows an output trend of $TENG_{FEP} > TENG_{Kapton} > TENG_{EC}$. The FEP is the most negative material, and thus generated the highest output. The EC lies toward the positive side of the triboelectric series, and the generation of less output suggests the positive behavior of MIL-88A. Figure 3D shows the surface potential generated on MIL-88A after hitting 60 times with FEP, Kapton, and EC (Kim et al., 2018). The positive signal suggests the development of positive potential on MIL-88A when hit with FEP and Kapton. The negative signal in EC's case suggests that MIL-88A develops negative surface potential when hit with EC. Thus MIL-88A is a positive triboelectric material concerning FEP and Kapton, whereas it is a negative triboelectric material regarding EC. The data comparing the MIL-88A with commonly used positive materials like paper, Al, and EC are shown in Figure S4. The MIL-TENG with FEP as the opposite layer is selected for further analysis. The working mechanism for vertical contact-separation MIL-TENG is shown in Figure S5. The TENG harnesses energy by employing the combined effect of contact electrification and electrostatic induction (Wang et al., 2016b; Hou et al., 2013). Figure S5A shows the device's initial state, where the top and bottom layers are separated at a maximum possible distance. This state is characterized by zero charge generation, a state with no potential difference. Figure S5B explains the fully pressed condition in which the top layer is in firm contact with the bottom layer. Equal and opposite charges developed on each layer. The MIL-88A gets positively charged as it is a positive triboelectric material in comparison with FEP. The layers try to return to their original position in the absence of force. A potential difference arises during the process, allowing the flow of electrons from the top Al electrode to the bottom Al electrode until the layers get fully separated (Figures S5C and S5D). This process generated the half cycle of the TENG AC output. When force is applied, vice versa happens; the top layer starts moving toward the bottom layer, allowing the flow of electrons from the bottom electrode to the top electrode (Figure S5E). This reverse flow of electrons adds the other half cycle to the TENG output. The dynamic periodic contact-separation process produces the output of the MIL-TENG device. Figures 3E and 3F illustrate the effect of frequency on the output of MIL-TENG. The output increases with an increase in frequency up to 1.3 Hz. The MIL-TENG produces a maximum output of 90 V and 2.5 μA at 1.3 Hz. The voltage and current output of the device increase with frequency increase due to more accumulation of the residual charges on the Al electrodes. With increases in frequency, the electrons flow externally and can quickly reach equilibrium (Song et al., 2016; Dudem et al., 2015). The non-uniformity in the output occurs at a frequency of 1.7 Hz due to the mismatch of the frequency of the excitation and frequency of the output wave (Song et al., 2016). The low-frequency motions can be possible to harness by using the MIL-TENG.

At higher resistance, the output characteristics of TENG is close to open-circuit (OC) conditions. In OC condition, the voltage saturates at V_{oc} (Niu et al., 2013). The MIL-TENG open-circuit voltage (V_{oc}) and its stability are shown in Figures 4A and S6A. The MIL-TENG achieved a V_{oc} of 98 V. The ability to maintain the constant output for a longer period is highly desirable for practical applications. Figures 4B and S6B depict the stability of the device. Furthermore, the output of the device was tested after 10 days (Figure S7). The negligible

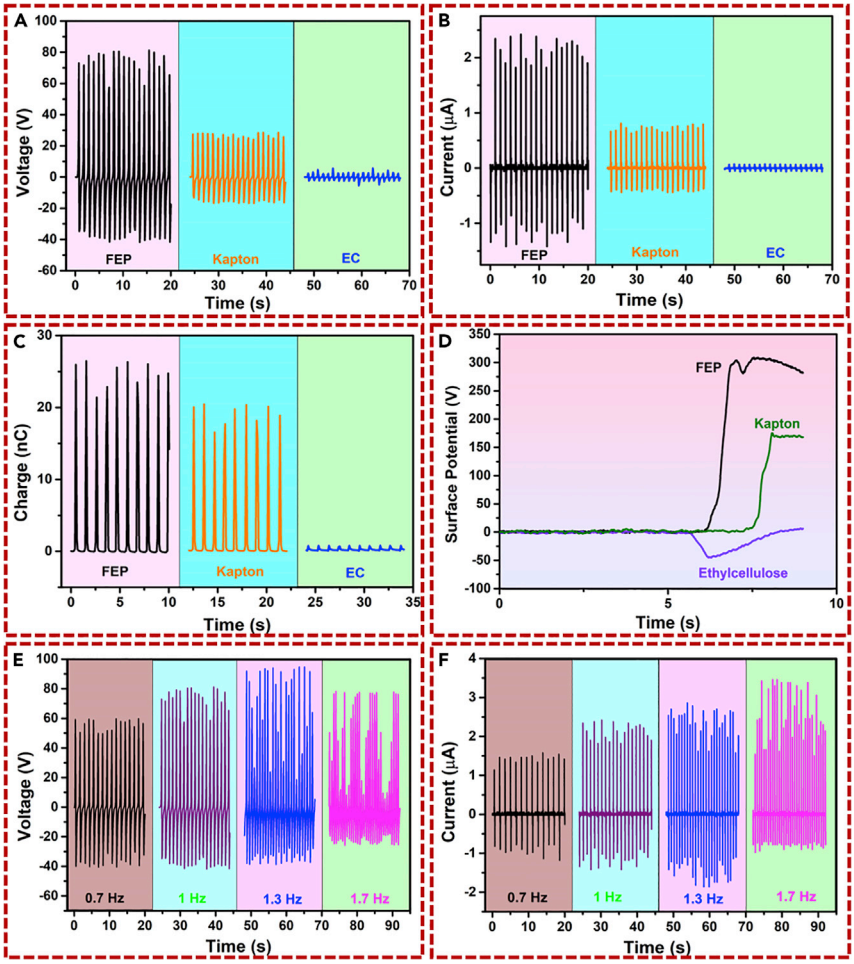

Figure 3. Electrical performance of MIL-TENG

(A–C) The produced (A) voltage, (B) current, and (C) charge profiles of MIL-TENG with FEP, Kapton, and ethylcellulose are opposite layers.

(D) Surface potential developed on MIL-88A after 60 contacts with FEP, Kapton, and ethylcellulose film.

(E and F) The (E) voltage and (F) current profiles of MIL-TENG (FEP) at various frequencies.

change in the output after 10 days confirmed the long-term environmental stability of the device. The load matching analysis to find the optimized power is critical for the applicability of the TENG. Figures 4C and 4D show the voltage, power, and power density across various loads ranging from 10 kΩ to 3 GΩ. The voltage increases with an increase in resistance, as generally observed in TENG. The MIL-TENG generated a maximum power and power density of 10.125 μW and 16.2 mW/m^2, respectively, across a load of 200 MΩ. The discontinuous AC output of TENG is not suitable for powering electronics. Thus, TENG's AC output was converted to DC output via a rectification circuit to charge numerous capacitors. Figure 4E shows the capacitor charging profile for 0.22-, 0.5-, and 1-μF capacitors. The charging time increases with an increase in capacitance. The energy stored in the capacitors is shown in Figure S8. The charge and self-discharge cycle for 1-μF capacitor is shown in Figure 4F. The capacitor exhibits a stable charge-discharge cycle.

The harvesting of motions generated during individual daily activities is a great mechanical energy source to drive TENG. Figures 5A and 5B show the utilization of various biomechanical motions like finger tapping, hand tapping, and leg tapping for energy harnessing via MIL-TENG. The image of the device used for the purpose is shown in Figure S9. Moreover, the output generated at fast hand tapping and jogging are illustrated in Figure 5C. The device is suitable to harvest slow as well as fast body movements. Finally, MIL-TENG is demonstrated for consumer and practical implementation. The device's practical implementation was demonstrated by powering numerous electronics via a 50-μF capacitor charged using two

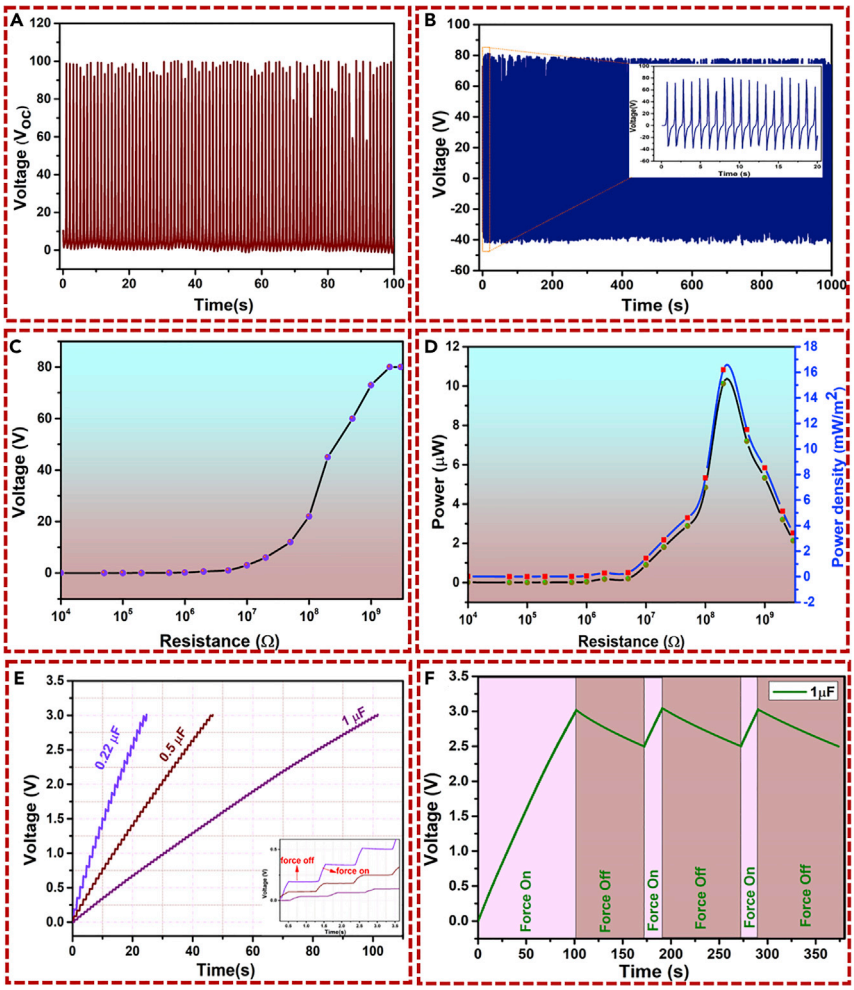

Figure 4. Electrical performance of MIL-TENG

(A) The open-circuit voltage versus time graph of MIL-TENG.

(B) The stability of MIL-TENG for 1000 s.

(C) The voltage generated by MIL-TENG across various resistances.

(D) Power and power density of MIL-TENG across a series of resistances.

(E and F) (E) The charging profile of 0.22-, 0.5-, and 1-μF capacitor and (F) the behavior of 1-μF capacitor during charge and self-discharge cycles.

MIL-TENG devices. Figure 5D depicts the charging profile of 50-μF capacitor. Figures 5E–5G shows the powering up of wristwatch, stopwatch, and calculator using 50-μF capacitor. The detailed images with capacitor and rectifier connecting with the electronics are shown in Figure S10. The wristwatch, stopwatch, and calculator are powered up for 42 s, 3 s and 8 s, respectively. The signal after turning on the switch for the wristwatch, stopwatch, and calculator is shown in Figure S11.

Conclusion

In summary, we instigate a biodegradable MOF MIL-88A for vertical contact-separation mode triboelectric nanogenerator. The MIL-TENG was developed with FEP, Kapton, and ethylcellulose as an opposite layer. The MIL-88A behaves as a positive material concerning FEP and Kapton and negative material regarding ethylcellulose. The MIL-88A/FEP produced a voltage, current, and charge of 80 V, 2.2 μA, and 25 nC, respectively. The as-fabricated device was demonstrated for biomechanical energy harvesting to harness different hand and leg motions. Moreover, several low-rating electronics like calculator, stopwatch, and wristwatch are powered via a capacitor charged using MIL-TENG device. The results confirm the use of biodegradable MOF for TENG, which will extend the utilization of MOFs for future implantable and biodegradable devices.

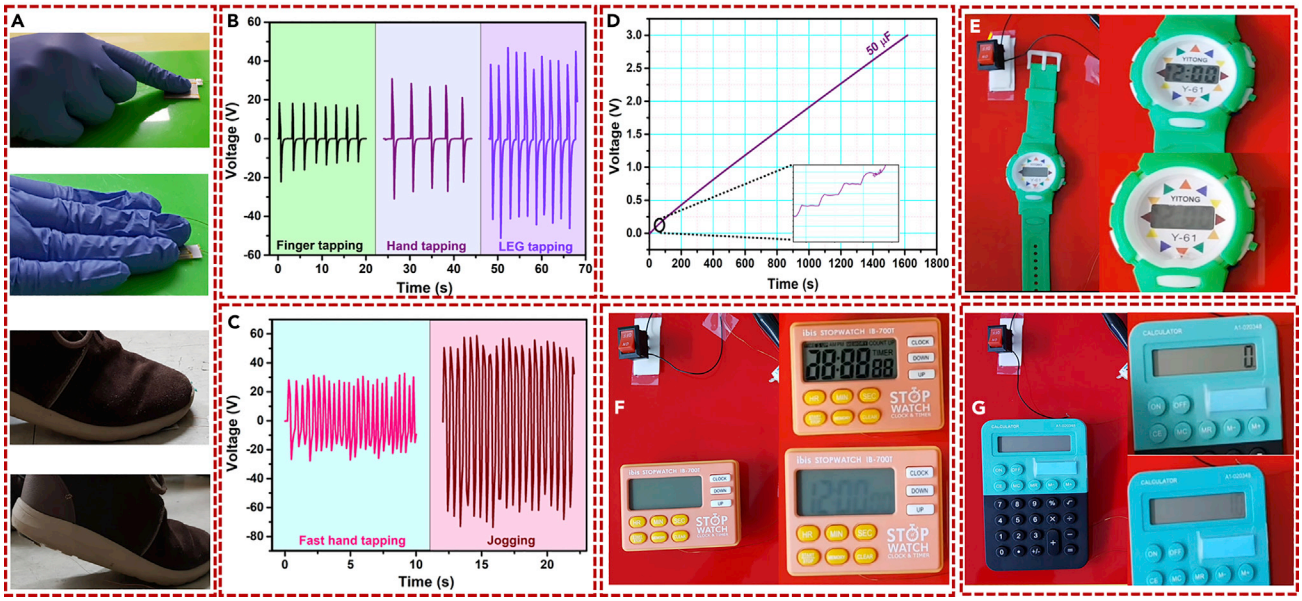

Figure 5. Biomechanical energy harvesting and driving low-power electronics

(A) The numerous biomechanical motions used for harnessing energy via MIL-TENG.

(B) The electrical output of MIL-TENG generated during finger, hand, and leg tapping.

(C) The electrical output of MIL-TENG generated during fast hand tapping and jogging.

(D–G) (D) The charging of 50-μF capacitors to power the (E) wristwatch, (F) stopwatch, and (G) calculator.

Limitations of the study

Our work has reported the biodegradable MOF MIL-88A for TENG. Although the fabricated device is stable and has good performance, biodegradable materials can be extended by fabricating the biodegradable device. Therefore, soon, we will work on the growth or the coating of biodegradable MOFs on conducting foils like Mg for the eco-friendly, biodegradable devices and sensors.

Resource availability

Lead contact

Sang-Jae Kim (kimsangj@jejunu.ac.kr).

Materials availability

Materials used in the study are commercially available.

Data and code availability

This study did not generate computer code. All data and analytical methods are available in the main text or in Supplemental information section.

METHODS

All methods can be found in the accompanying Transparent methods supplemental file.

SUPPLEMENTAL INFORMATION

Supplemental Information can be found online at https://doi.org/10.1016/j.isci.2021.102064.

ACKNOWLEDGMENTS

This work was supported by the Basic Science Research Program through the National Research Foundation of Korea (NRF) grant funded by the Korean government (MSIT) (2019R1A2C3009747, 2021R1A4A2000934).

AUTHOR CONTRIBUTIONS

G.K. designed, developed, and performed the experiments. N.P.M.J.R. and V.V. assisted in surface potential measurement and data analysis. G.K. wrote the paper. S.-J.K., funding acquisition, supervision, and manuscript corrections. All authors discussed the results and commented on the manuscript.

DECLARATION OF INTERESTS

There is no conflict of interest to declare.

Received: October 7, 2020
Revised: December 3, 2020
Accepted: January 11, 2021
Published: February 19, 2021

REFERENCES

Baati, T., Njim, L., Neffati, F., Kerkeni, A., Bouttemi, M., Gref, R., Najjar, M.F., Zakhama, A., Couvreur, P., Serre, C., and Horcajada, P. (2013). In depth analysis of the in vivo toxicity of nanoparticles of porous iron(iii) metal–organic frameworks. Chem. Sci. *4*, 1597–1607.

Baumann, A.E., Burns, D.A., Liu, B., and Thoi, V.S. (2019). Metal-organic framework functionalization and design strategies for advanced electrochemical energy storage devices. Commun. Chem. *2*, 86.

Dudem, B., Ko, Y.H., Leem, J.W., Lee, S.H., and Yu, J.S. (2015). Highly transparent and flexible triboelectric nanogenerators with subwavelength-architectured polydimethylsiloxane by a nanoporous anodic aluminum oxide template. ACS Appl. Mater. Inter. *7*, 20520–20529.

Durymanov, M., Permyakova, A., Sene, S., Guo, A., Kroll, C., Giménez-Marqués, M., Serre, C., and Reineke, J. (2019). Cellular uptake, intracellular trafficking, and stability of biocompatible metal-organic framework (MOF) particles in Kupffer cells. Mol. Pharmaceutics *16*, 2315–2325.

Furukawa, H., Cordova, K.E., O'keeffe, M., and Yaghi, O.M. (2013). The chemistry and applications of metal-organic frameworks. Science *341*, 1230444.

Guo, Y., Cao, Y., Chen, Z., Li, R., Gong, W., Yang, W., Zhang, Q., and Wang, H. (2020). Fluorinated metal-organic framework as bifunctional filler toward highly improving output performance of triboelectric nanogenerators. Nano Energy *70*, 104517.

Hou, T.-C., Yang, Y., Zhang, H., Chen, J., Chen, L.-J., and Lin Wang, Z. (2013). Triboelectric nanogenerator built inside shoe insole for harvesting walking energy. Nano Energy *2*, 856–862.

Jeong, C.K., Baek, K.M., Niu, S., Nam, T.W., Hur, Y.H., Park, D.Y., Hwang, G.-T., Byun, M., Wang, Z.L., Jung, Y.S., and Lee, K.J. (2014). Topographically-designed triboelectric nanogenerator via block copolymer self-assembly. Nano Lett. *14*, 7031–7038.

Khandelwal, G., Chandrasekhar, A., Maria Joseph Raj, N.P., and Kim, S.-J. (2019). Metal–organic framework: a novel material for triboelectric nanogenerator–based self-powered sensors and systems. Adv. Energy Mater. *9*, 1803581.

Khandelwal, G., Maria Joseph Raj, N.P., and Kim, S.-J. (2020a). Zeolitic imidazole framework: metal–organic framework subfamily members for triboelectric nanogenerators. Adv. Funct. Mater. *30*, 1910162.

Khandelwal, G., Maria Joseph Raj, N.P., and Kim, S.-J. (2020b). ZIF-62: a mixed linker metal–organic framework for triboelectric nanogenerators. J. Mater. Chem. A *8*, 17817–17825.

Kim, D.W., Kim, S.-W., and Jeong, U. (2018). Lipids: source of static electricity of regenerative natural substances and nondestructive energy harvesting. Adv. Mater. *30*, 1804949.

Lee, S., Lee, Y., Kim, D., Yang, Y., Lin, L., Lin, Z.-H., Hwang, W., and Wang, Z.L. (2013). Triboelectric nanogenerator for harvesting pendulum oscillation energy. Nano Energy *2*, 1113–1120.

Li, H., Wang, K., Sun, Y., Lollar, C.T., Li, J., and Zhou, H.-C. (2018). Recent advances in gas storage and separation using metal–organic frameworks. Mater. Today *21*, 108–121.

Liao, X., Wang, F., Wang, F., Cai, Y., Yao, Y., Teng, B.-T., Hao, Q., and Shuxiang, L. (2019). Synthesis of (100) surface oriented MIL-88A-Fe with rod-like structure and its enhanced fenton-like performance for phenol removal. Appl. Catal. B Environ. *259*, 118064.

Liu, N., Huang, W., Zhang, X., Tang, L., Wang, L., Wang, Y., and Wu, M. (2018). Ultrathin graphene oxide encapsulated in uniform MIL-88A(Fe) for enhanced visible light-driven photodegradation of RhB. Appl. Catal. B: Environ. *221*, 119–128.

Niu, S., Wang, S., Lin, L., Liu, Y., Zhou, Y.S., Hu, Y., and Wang, Z.L. (2013). Theoretical study of contact-mode triboelectric nanogenerators as an effective power source. Energy Environ. Sci. *6*, 3576–3583.

Song, Y., Cheng, X., Chen, H., Huang, J., Chen, X., Han, M., Su, Z., Meng, B., Song, Z., and Zhang, H. (2016). Integrated self-charging power unit with flexible supercapacitor and triboelectric nanogenerator. J. Mater. Chem. A *4*, 14298–14306.

Tang, W., Zhang, C., Han, C.B., and Wang, Z.L. (2014). Enhancing output power of cylindrical triboelectric nanogenerators by segmentation design and multilayer integration. Adv. Funct. Mater. *24*, 6684–6690.

Wang, J., Wan, J., Ma, Y., Wang, Y., Pu, M., and Guan, Z. (2016a). Metal–organic frameworks MIL-88A with suitable synthesis conditions and optimal dosage for effective catalytic degradation of Orange G through persulfate activation. RSC Adv. *6*, 112502–112511.

Wang, Z.L., Lin, L., Chen, J., Niu, S., and Zi, Y. (2016b). Triboelectric nanogenerator: vertical contact-separation mode. In Triboelectric Nanogenerators, Z.L. Wang, L. Lin, J. Chen, S. Niu, and Y. Zi, eds. (Springer International Publishing), pp. 23–47.

Wang, L., Zheng, M., and Xie, Z. (2018). Nanoscale metal–organic frameworks for drug delivery: a conventional platform with new promise. J. Mater. Chem. B *6*, 707–717.

Wen, R., Guo, J., Yu, A., Zhai, J., and Wang, Z.L. (2019). Humidity-resistive triboelectric nanogenerator fabricated using metal organic framework composite. Adv. Funct. Mater. *29*, 1807655.

Zhai, L., Cui, S., Tong, B., Chen, W., Wu, Z., Soutis, C., Jiang, D., Zhu, G., and Mi, L. (2020). Bromine-functionalized covalent organic frameworks for efficient triboelectric nanogenerator. Chem. A Eur. J. *26*, 5784–5788.

iScience, Volume *24*

Supplemental Information

Biodegradable metal-organic framework

MIL-88A for triboelectric nanogenerator

Gaurav Khandelwal, Nirmal Prashanth Maria Joseph Raj, Venkateswaran Vivekananthan, and Sang-Jae Kim

Supplemental Information

Biodegradable Metal-Organic Framework MIL-88A for Triboelectric Nanogenerator

Gaurav Khandelwal,[1] Nirmal Prashanth Maria Joseph Raj,[1] Vivekananthan Venkateswaran,[1] Sang-Jae Kim,[1*]

[1] Nanomaterials and System Lab, Faculty of Applied Energy Systems, Major of Mechatronics Engineering, Jeju National University, Jeju 690-756, South Korea

[*] Corresponding Author and Lead Contact, Email: kimsangj@jejunu.ac.kr

Transparent Methods

Experimental

1. **Materials:** Iron chloride hexahydrate ($FeCl_3.6H_2O$) and fumaric acid were purchased from Daejung Chemicals Ltd. (South Korea). Ethylcellulose (48% ethoxy content) was purchased from Acros organics (USA).
2. **Synthesis of MIL-88A:** MIL-88A was synthesized using a procedure reported by Liao et al. (Liao et al., 2019). Briefly, 1.352 g of $FeCl_3.6H_2O$ and 0.580 g of fumaric acid was dissolved in 25 ml of deionized (DI) water. The solution was transferred to a Teflon-lined stainless-steel autoclave and placed at a temperature of 65 °C for 4 h. The product was collected and washed several times with DI water, followed by drying.
3. **Device Fabrication:** The MIL-TENG was fabricated in a vertical contact-separation mode with an active area of 2.5 cm X 2.5 cm. MIL-88A was attached uniformly on a conducting adhesive aluminum tape (3M). The excess material was removed with the help of air gun. The MIL-88A attached Al tape was fixed on a polyethylene terephthalate (PET) substrate. The commercial FEP (50 µm) and Kapton (50 µm) films were directly attached to the aluminum tape followed by the PET substrate's attachment. The 10 wt% (1:4 ethanol: toluene) ethyl cellulose solution was spin-coated on the Al tape followed by the PET substrate's attachment. The copper wires were attached to the electrode using a silver paste for collecting output. Finally, the MIL-TENG was assembled by attaching the MIL-88A and opposite layers using a spacer.
4. **Characterization:** The XRD measurements were performed using Malvern PANalytical Empyrean, with a generator voltage and tube current of 40 V and 30 mA, respectively. FT-IR measurements were taken on the Bruker Alpha II compact FT-IR spectrometer. The surface morphology image and EDS mapping were taken on Tescan MIRA-3 FE-SEM provided with Oxford EDS detector. The surface roughness analysis

was carried out using the NanoSystem NV2200 3D surface profiler. All the electrical measurements were performed under lab-made Faraday cage to reduce the noise. The force was applied using a LinMot Inc. linear motor. A Keithley 6514 electrometer was used to measure the voltage and charge of the MIL-TENG device. A Stanford Research SR570 low noise current preamplifier and Tektronix mixed domain oscilloscope MDO3000 series was used for the MIL-TENG device's current measurement. The trek 347 non-contact electrostatic voltmeter was used to measure the surface potential developed on MIL-88A.

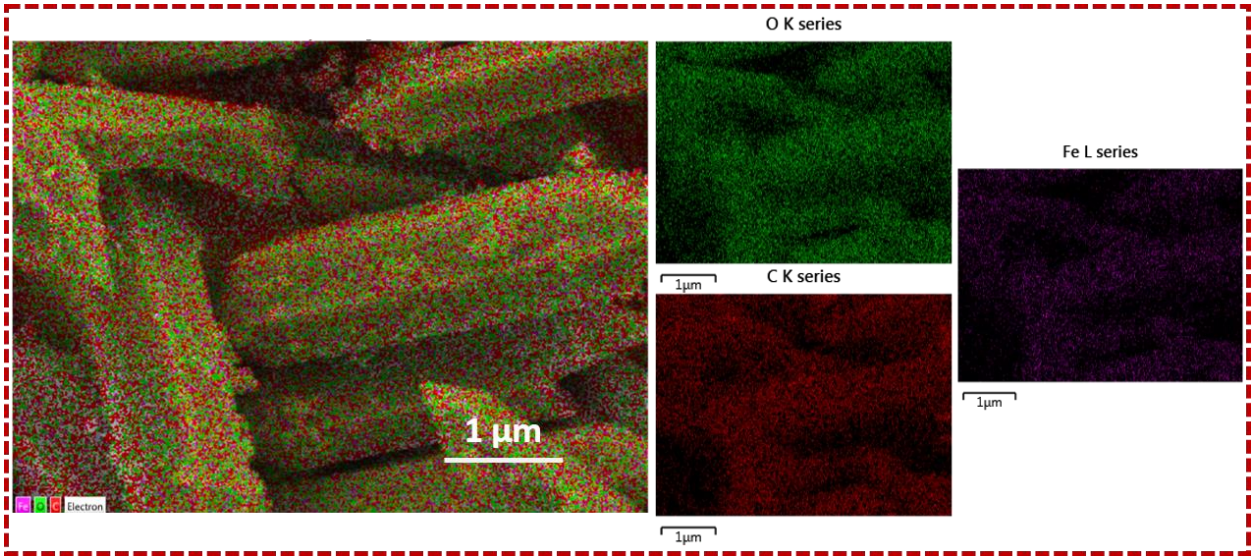

Figure S1. EDS elemental mapping for MIL-88A. (Related to Figure 1).

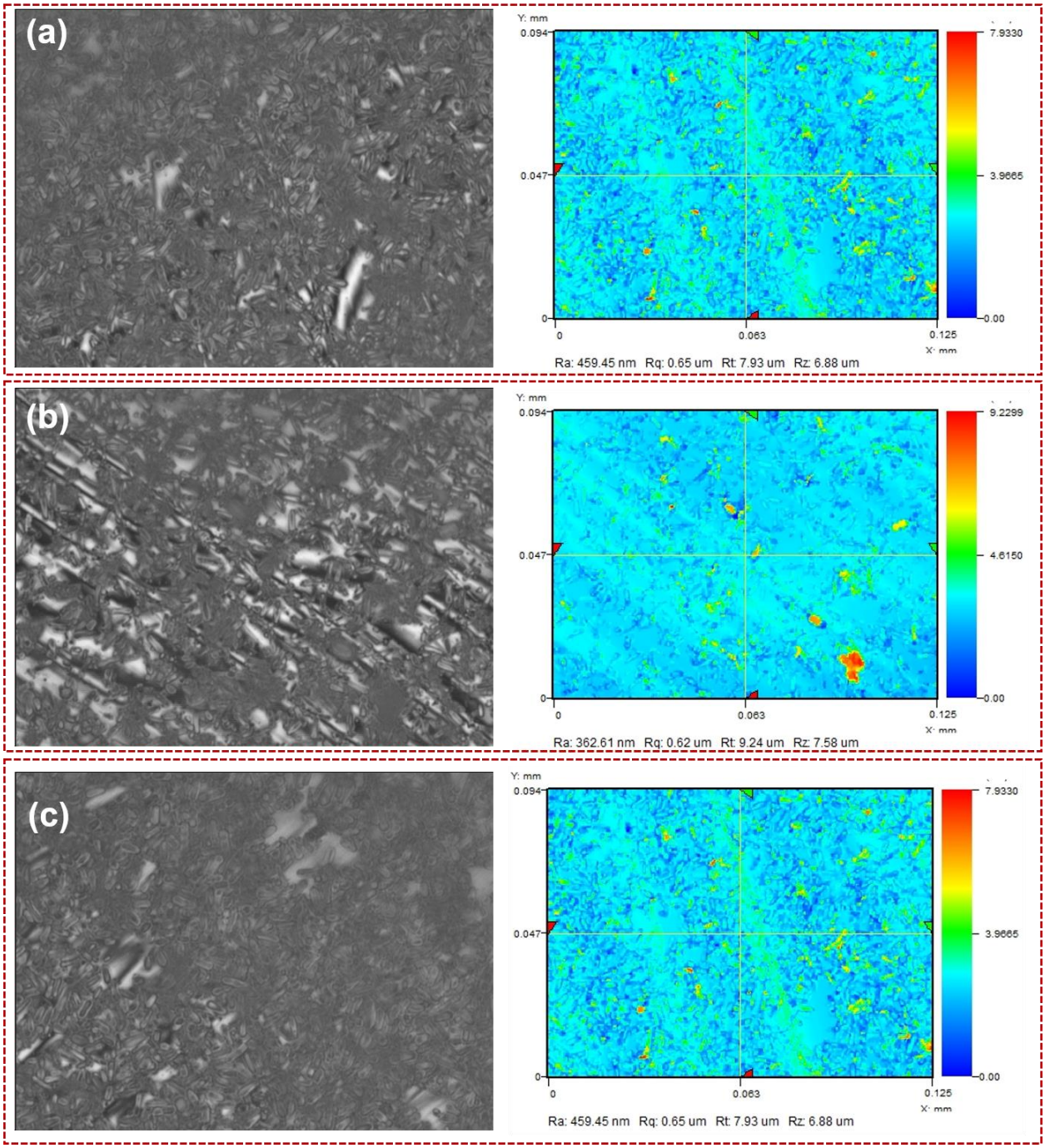

Figure S2. The optical and 2D profile images of the dispersed samples (Related to Figure 1).

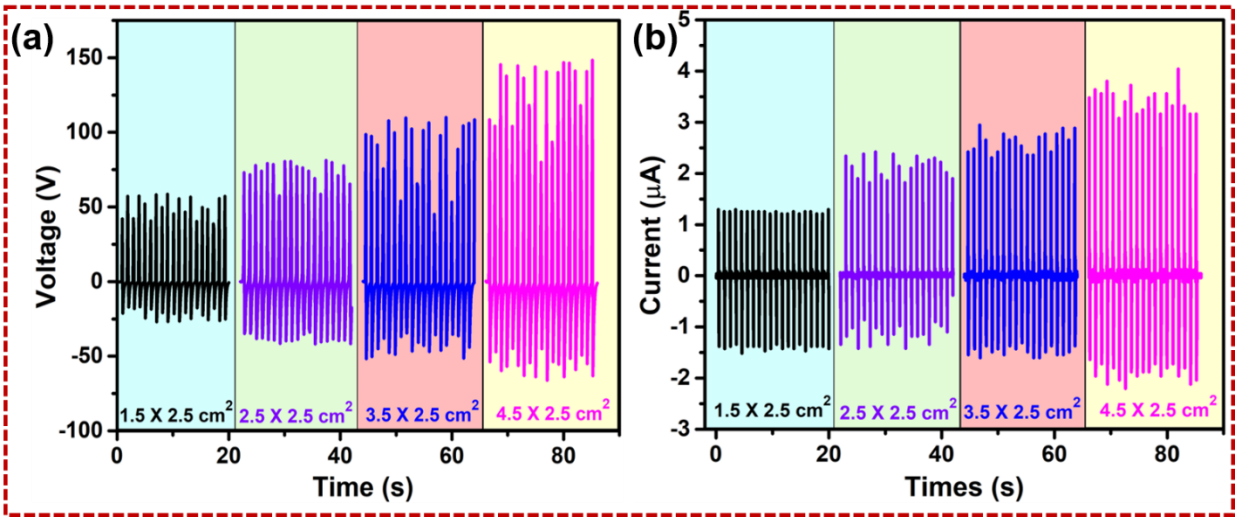

Figure S3. Voltage and current variation with the device size (Related to Figure 3).

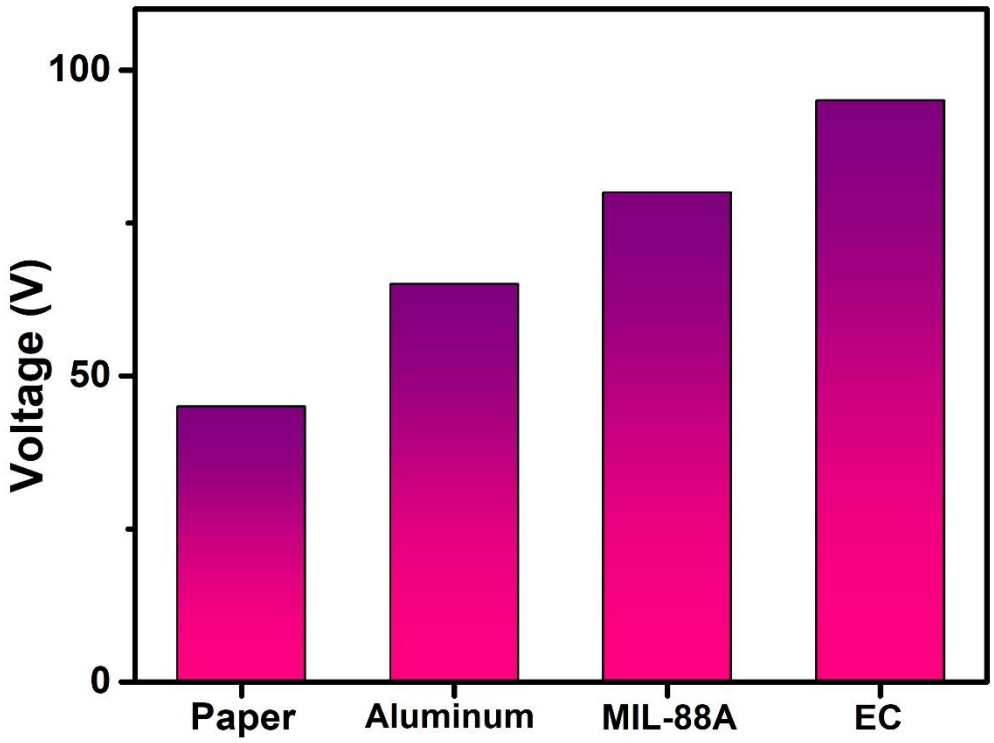

Figure S4. The comparison of voltage output generated by commonly used positive materials with MIL-88A (Related to Figure 3)

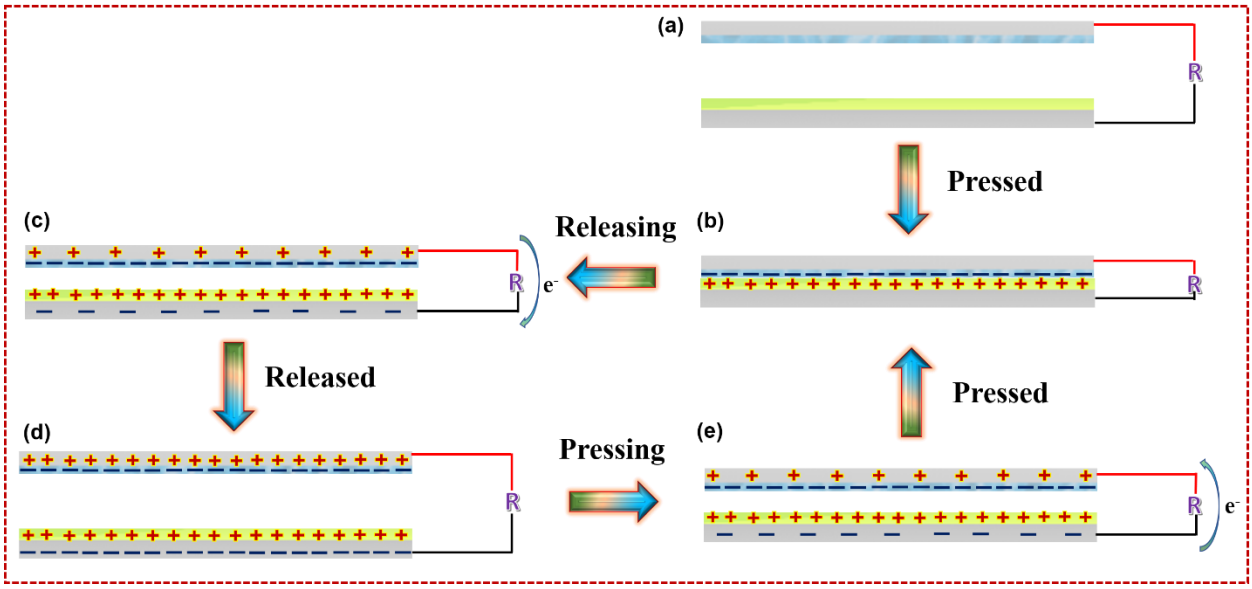

Figure S5. The schematic illustration of MIL-TENG working mechanism showing pressed, releasing, released and pressing conditions (Related to Figure 3).

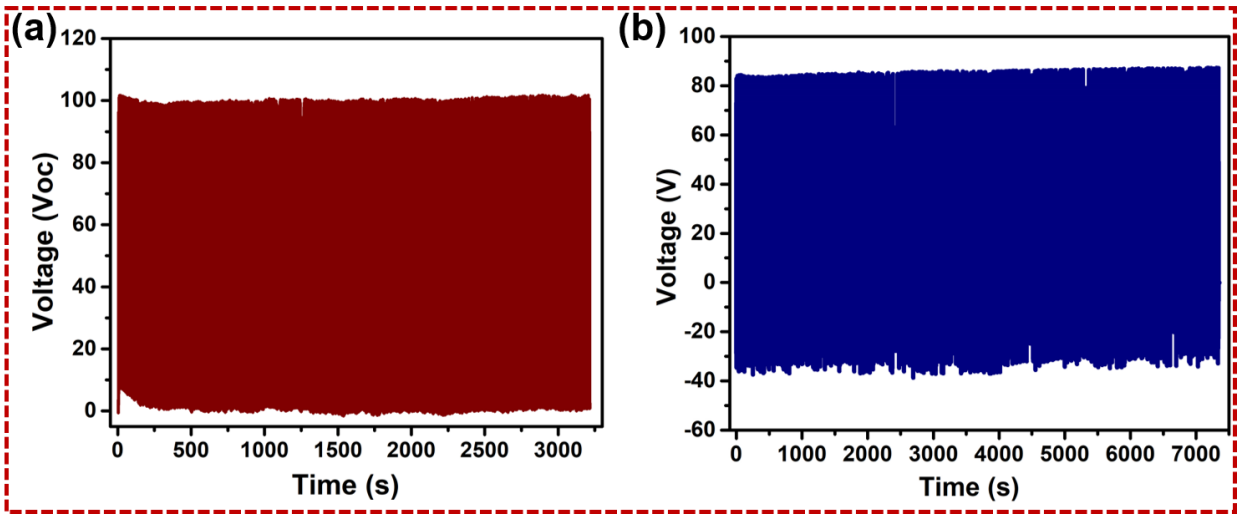

Figure S6. Stability of the device (Related to Figure 4).

(a) The stability of the open-circuit voltage and (b) long-term device stability.

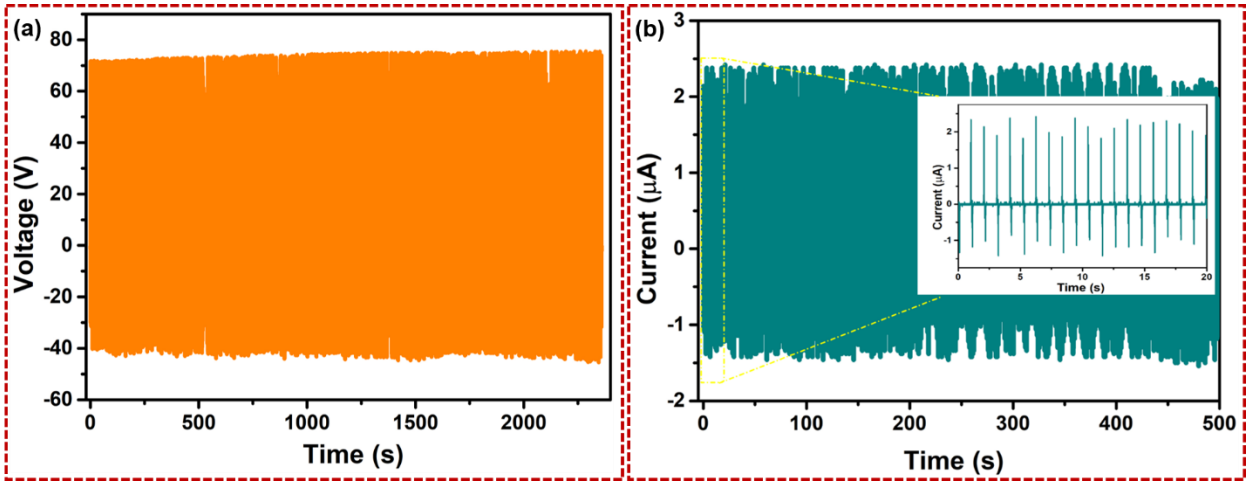

Figure S7. Voltage and current stability of MIL-TENG after 10 days (Related to Figure 4).

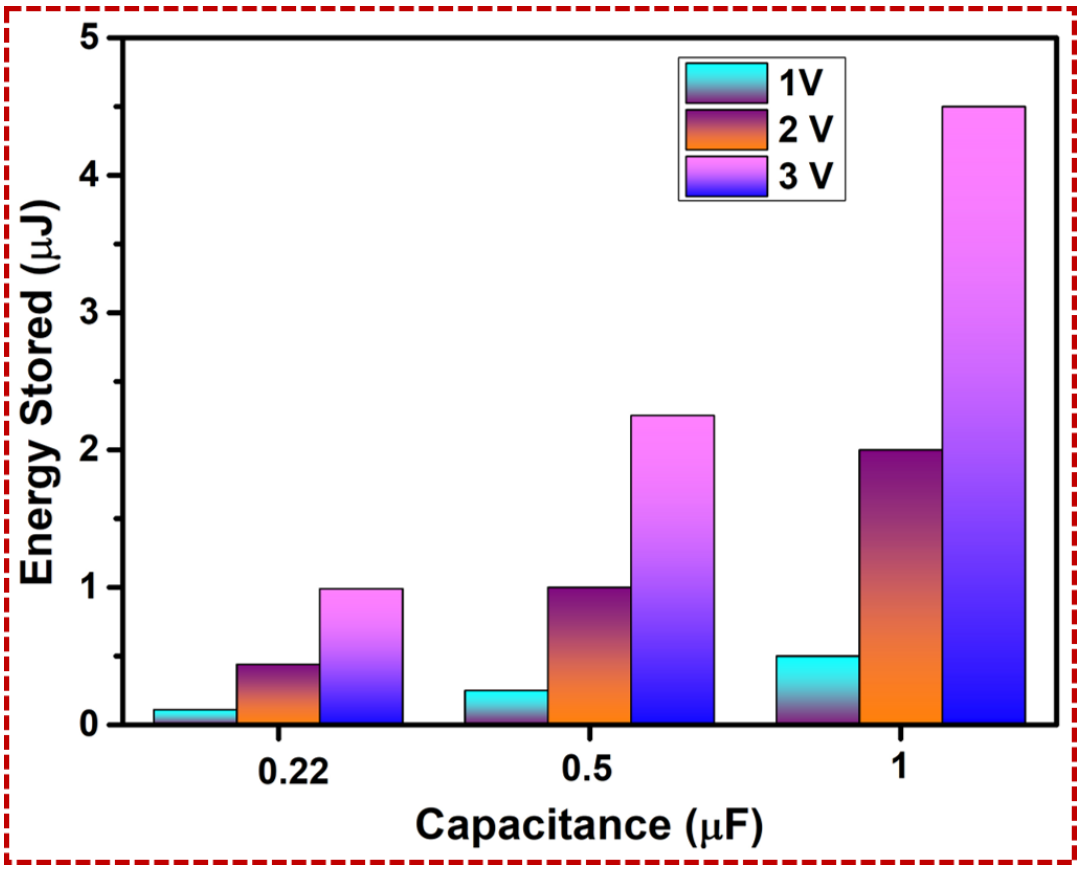

Figure S8. The energy stored in 0.22, 0.5 and 1 μF capacitor corresponding to 1, 2 and 3 V charging (Related to Figure 4).

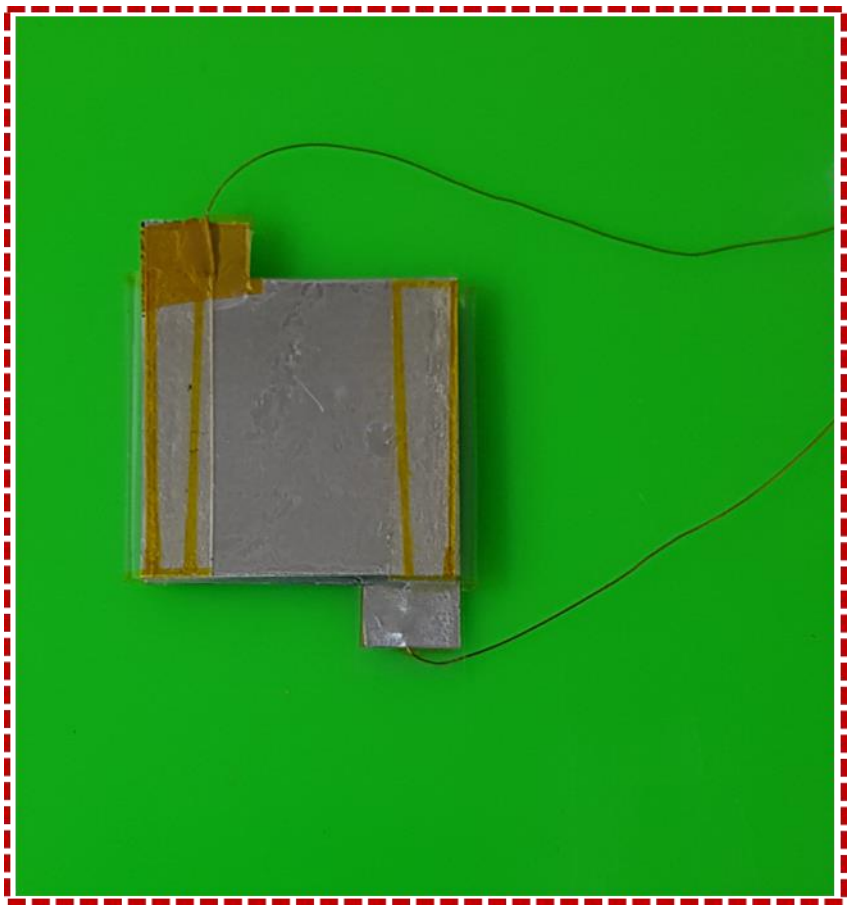

Figure S9. The image of the device used to power up the electronics via a capacitor (Related to Figure 5).

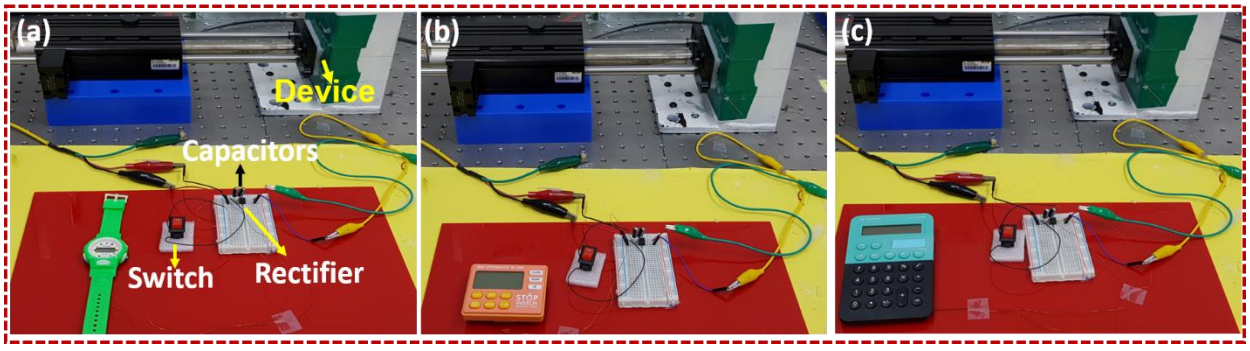

Figure S10. The detailed depiction of the electronics connected to the capacitor and rectifier (Related to Figure 5).

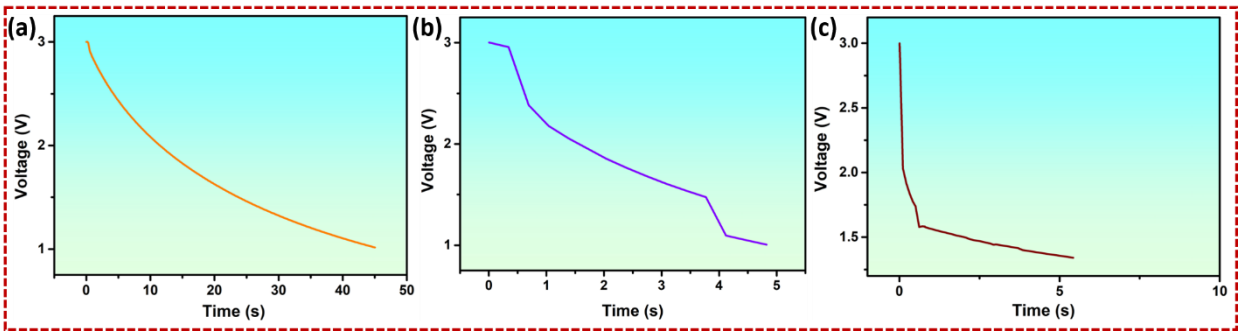

Figure S11. The capacitor discharge signal after turning on the switch to power up the electronics (Related to Figure 5).